



Cite this article: Chakraborty S, Goswami S, Quah CK, Pakhira B. 2018 Sensing study of quinoxaline analogues with theoretical calculation, single-crystal X-ray structure and real application in commercial fruit juices.

R. Soc. open sci. **5**: 180149.

<http://dx.doi.org/10.1098/rsos.180149>

Received: 12 February 2018

Accepted: 18 April 2018

Subject Category:

Chemistry

Subject Areas:

crystallography/supramolecular chemistry

Keywords:

chemosensors, nickel, iron(iii), crystal

Author for correspondence:

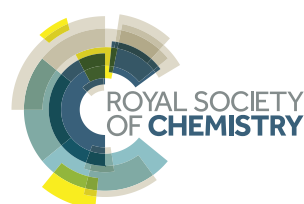
Shyamaprosad Goswami

e-mail: spgoswamical@yahoo.com

[†]Present address: Waste Water Technology Division, National Engineering Research Institute, Nagpur 440020, India.

This article has been edited by the Royal Society of Chemistry, including the commissioning, peer review process and editorial aspects up to the point of acceptance.

Electronic supplementary material is available online at <https://dx.doi.org/10.6084/m9.figshare.c.4102124>.



Sensing study of quinoxaline analogues with theoretical calculation, single-crystal X-ray structure and real application in commercial fruit juices

Shampa Chakraborty^{1,†}, Shyamaprosad Goswami¹,
Ching Kheng Quah² and Bholanath Pakhira¹

¹Department of Chemistry, Indian Institute of Engineering Science and Technology, Shibpur, Howrah, West Bengal 711103, India

²X-ray Crystallography Unit, School of Physics, Universiti Sains Malaysia, 11800 USM, Penang, Malaysia

SC, 0000-0001-7176-1542

Single-crystal X-ray structures of dimeric quinoxaline aldehyde (QA), quinoxaline dihydrazone (DHQ) and HQNM (Goswami S *et al.* 2013 *Tetrahedron Lett.* **54**, 5075–5077. (doi:10.1016/j.tetlet.2013.07.051); Goswami S *et al.* 2014 *RSC Adv.* **4**, 20922–20926. (doi:10.1039/C4RA00594E); Goswami S *et al.* 2014 *New J. Chem.* **38**, 6230–6235. (doi:10.1039/C4NJ01498G)) are reported along with the theoretical study. Among them, QA is not acting as an active probe, but DHQ and HQNM are serving as selective and sensitive probe for the Fe³⁺ cation and the Ni²⁺ cation, respectively. DHQ can also detect the Fe³⁺ in commercial fruit juices (grape and pomegranate).

1. Introduction

The design of a colorimetric cation sensor is important and useful because the colorimetric sensing system would allow ‘naked-eye’ detection of cations without the use of any spectroscopic instrumentation, being simple and convenient for detection. In particular, ratiometric sensors have the important feature of permitting signal rationing, and increase the dynamic range and provide built-in correction for the environmental effect. Such colorimetric/ratiometric receptors would be more

valuable if they can be obtained by a simple synthetic method. The important biological activities of quinoxaline derivatives [1–7] include anti-cancer, [8] antimicrobial/anti-tubercular [9], anti-protozoal [10], antiviral [11], inhibition of the enzyme phosphodiesterase [12] anti-inflammatory [13], anti-oxidant [13], anti-tumour and anti-hyperglycaemic activity, etc. Quinoxaline derivatives are known for their cancer chemopreventive effect [8]. Furthermore, the quinoxaline ring is a core structure of several drug molecules and acceptors such as clofazimine, echinomycin and actinomycin [14–17]. Recently, we have also reported some quinoxaline-based colorimetric and ratiometric sensors for specific detection of nickel cations [18–20]. Nickel is a toxic metal and known to cause pneumonitis, asthma and cancer of the lungs, and also disorders of the respiratory and the central nervous system [17,21–24]. Nickel is an essential trace element in biological systems with relevance to the biosynthesis and metabolism in certain microorganisms and plants. Nickel is used in various industries, e.g. in Ni–Cd batteries, rods for arc welding, pigments for paints, ceramics, electroplating, dental and surgical prostheses, and catalysts for hydrogenation, and as magnetic tapes of computers. On the other hand, iron is one of the essential elements for fulfilling physiological function in the human body. Iron plays key roles in various important biological processes at the cellular level, ranging from electron transfer, cellular metabolism, energy generation, gene expression, neurotransmission, regulation of metalloenzymes, DNA synthesis as well as differentiation [25,26]. In particular, its deficiency or overload can cause various disorders and diseases such as anaemia and haemochromatosis. Thus, the development of the sensitive and selective detection approaches of Fe^{3+} in biological systems is of great importance for investigating the physiological and pathological functions of Fe^{3+} in living organisms. In this paper, we investigate the behaviour of three quinoxaline-based derivatives where they act as an active sensor for metal cations and also its real-world application in detection of iron in fruit juices.

2. Results and discussion

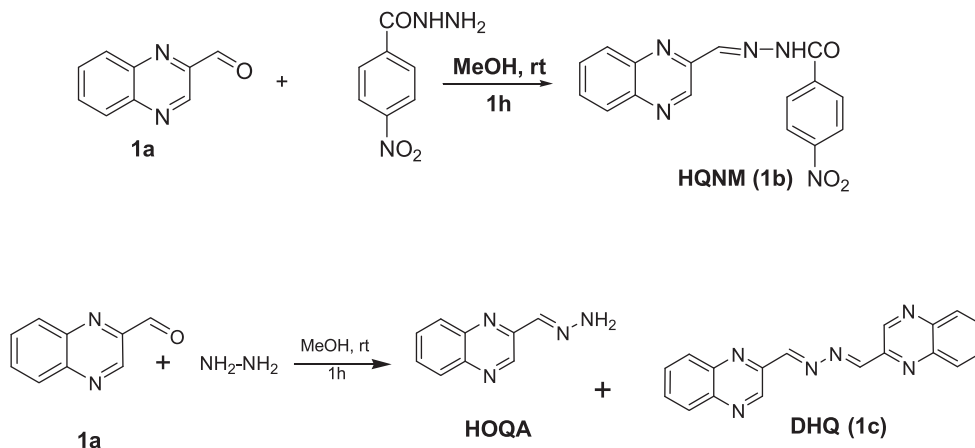
The design and synthesis of sensors for the detection of a selective metal ion in an aqueous or non-aqueous medium is an active area of research today. Colorimetric sensors are important due to their simplicity and lower capital cost compared with the other closely related methods. Accordingly, the development of a novel colorimetric chemosensor for the rapid and convenient detection of Ni^{2+} and Fe^{3+} is attractive. The binding behaviour of receptor (HQNM) [18] has already been established, hence, in this article, we are discussing more about DHQ and its sensing behaviour with different cations.

The titration was carried out in CH_3CN -HEPES buffer (9:1, v/v, pH=7.4) at a 1×10^{-5} M concentration of HQNM and DHQ upon addition of incremental amounts of 0–200 μl of nickel chloride solution (2×10^{-4} M) and ferric chloride solution (2×10^{-4} M), respectively (schemes 1 and 2).

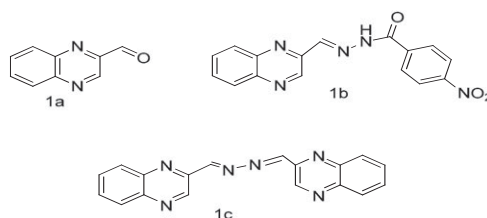
The UV-visible spectrum of the receptor HQNM [18] with Ni^{2+} is characterized by two bands centred at 340 and 442 nm (figure 1). As shown in figure 1a, upon gradually increasing the nickel ion concentration, the band at 340 nm gradually weakens and a new band appears at 442 nm with an isosbestic point at 370 nm. The UV-visible spectrum of the DHQ and Fe^{3+} is shown in figure 1b; it was also characterized by three bands centred at 239, 312 and 361 nm. Upon gradually increasing the iron ion concentration, a gradual increase of each band in the UV-visible spectrum is seen. The UV-visible spectrum of DHQ with commercial grape and pomegranate juices is also shown in figure 1c and 1d, respectively. In figure 1c, upon gradually increasing the grape juice concentration (20 μl), the band at 275 nm gradually increases. Similarly in figure 1d, upon gradually increasing the pomegranate juice concentration (20 μl), the band at 275 nm gradually increases. Thus the UV-vis absorption spectra of Fe^{3+} in fruit juices could be detected and estimated [27–30] in an aqueous medium and in commercial fruit juice. A control experiment without receptor and only CH_3CN -HEPES buffer (9:1, v/v, pH=7.4) with fruit juices has been carried out without any significant enhancement of absorbance (electronic supplementary material, figure S9a and S9b).

The selectivity for the ferric ion over the other cations is shown by plotting the UV-vis spectra diagram of DHQ with different cations. In figure 2, the selectivity for Fe^{3+} is shown by the brown spectrum. However, when titration of other cations such as Ni^{2+} , Cu^{2+} , Cd^{2+} , Zn^{2+} , Na^+ , K^+ , Mn^{2+} , Hg^{2+} was performed in similar experimental conditions, no significant change in the spectrum for most of the cations was noted except for Co^{2+} and Fe^{2+} , but the colour change for those metal cations is not detectable with the naked eye.

From the experimental data, it can be concluded that the receptor DHQ possesses high selectivity and sensitivity towards the iron (III) cation in acetonitrile–HEPES buffer (9:1, v/v, pH=7.4) medium. The other cations had no practical significant influence. The colour changes are most probably due to



Scheme 1. Brief synthesis of the HQNM (1b) and DHQ (1c) from QA (1a).



Scheme 2. Chemical structures of (1a) QA (1b) HQNM (1c) Quinoxaline DHQ.

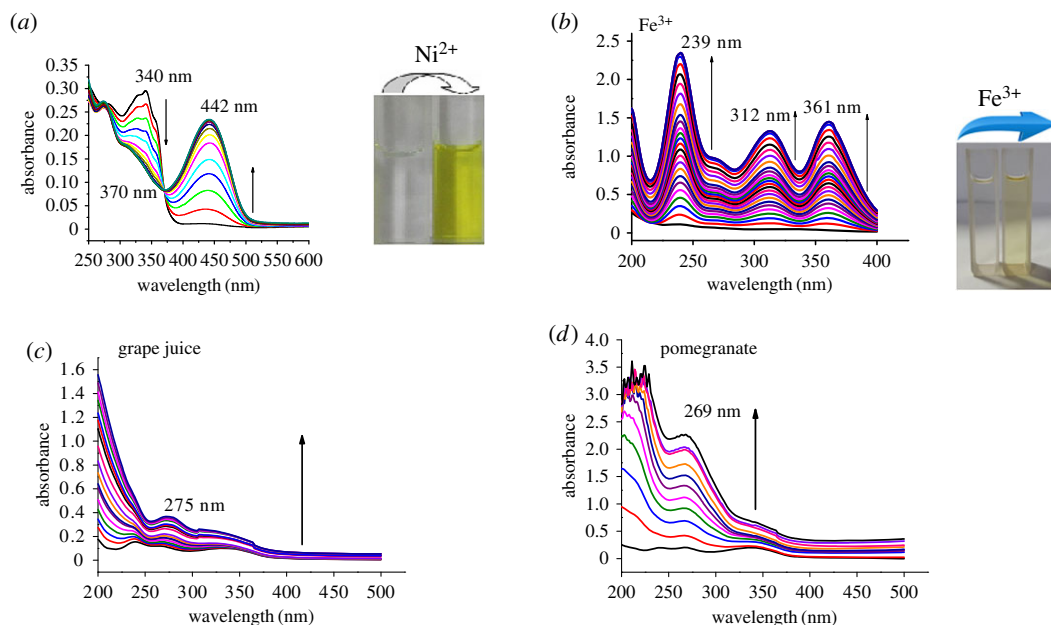


Figure 1. (a) UV-vis absorption spectra of HQNM (1×10^{-5} M) in CH₃CN-HEPES buffer (9 : 1, v/v, pH = 7.4) upon titration with nickel chloride (NiCl₂·6H₂O, 0.8 equivalent). The arrows show changes due to the increasing concentration of Ni²⁺. Inset: colour change due to the addition of nickel chloride. (b) UV-vis absorption spectra of DHQ (1×10^{-5} M) in CH₃CN-HEPES buffer (9 : 1, v/v, pH = 7.4) upon titration with ferric chloride (FeCl₃·6H₂O, 0.8 equivalent). The arrows show changes due to the increasing concentration of Fe³⁺. Inset: colour change due to the addition of ferric chloride. (c) UV-vis absorption spectra of DHQ (1×10^{-5} M) in CH₃CN-HEPES buffer (9 : 1, v/v, pH = 7.4) upon titration with commercial grape juice. The arrows show changes due to the increasing concentration of Fe³⁺. (d) UV-vis absorption spectra of DHQ (1×10^{-5} M) in CH₃CN-HEPES buffer (9 : 1, v/v, pH = 7.4) upon titration with commercial pomegranate juice. The arrows show changes due to the increasing concentration of Fe³⁺.

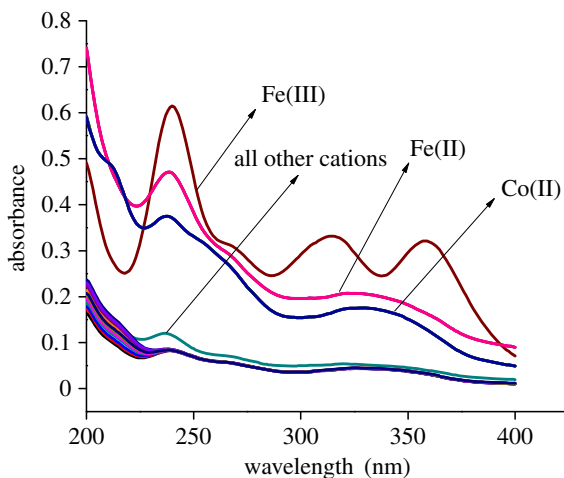
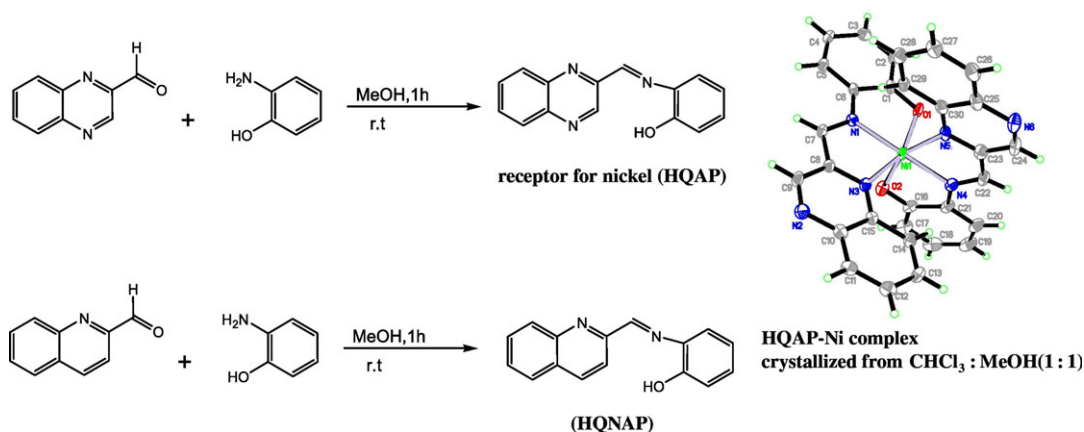


Figure 2. The absorption spectra of DHQ (1×10^{-5} M) and DHQ with all other cations (2×10^{-4} M) in acetonitrile–HEPES buffer (9 : 1, v/v, pH = 7.4).

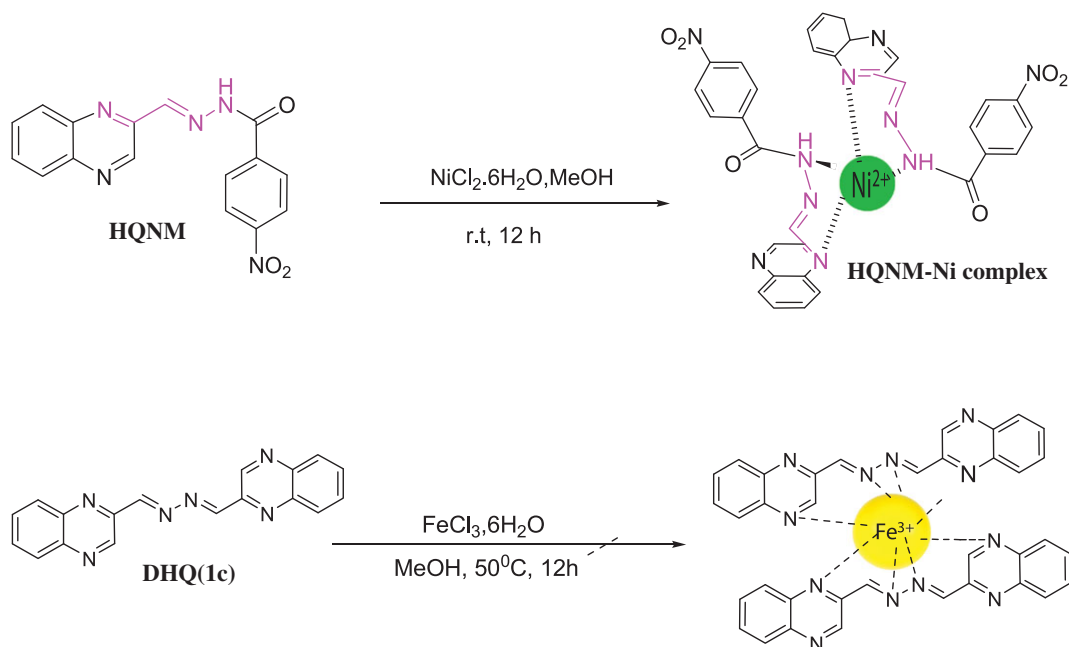


Scheme 3. Synthesis of the receptor (HQAP) and HQNAP.

the formation of coordinate bonds of receptor DHQ on the addition of the ferric ion, which is shown in figure 1*b* (inset).

To further explore the binding mechanism, Job's plot of the UV–vis titrations of the Fe^{3+} ion with a total volume of 2 ml was revealed. Maximum absorption was observed when the molar fraction reached 0.65, which is indicative of a 2:1 stoichiometric complexation between DHQ and the Fe^{3+} ion for the newly formed species. The electrospray ionization (ESI) mass spectrum of a mixture of DHQ and $\text{FeCl}_3 \cdot 6\text{H}_2\text{O}$ also revealed the formation of a 2:1 ligand–metal complex through the metal coordination interaction, with a major signal at $m/z = 679.0$ (possibly for $(2\text{M} + \text{Fe})^+$ ions) (scheme 3).

The binding selectivity for HQNM (scheme 2 and figure 1*a*) is greatly influenced based on charge–charge interactions, and the involvement of both N–H ... Ni bonds, which are absent in the case of quinoxaline aldehyde (QA) and DHQ, as they already exist as dimers, as seen from their crystal structure (figure 2). In accordance with this discussion, for a similar type of compound acting as an active probe or not, two more examples from our previous work are HQNAP (quinoline-2-ylmethyleamine, scheme 2) and HQAP^{1b} (quinoxalin-2-ylmethyleamine). In contrast to our previous receptor HQAP [18], HQNAP does not serve as a good nickel sensor (electronic supplementary material, figure S8). Surprisingly, from the complex crystal structure of HQAP, we cannot see any direct bond with the second quinoxaline nitrogen to the nickel. However, from that fact we can say that there must be some effect of the second quinoxaline nitrogen on the HQAP–Ni complex so that it will be formed, and of the quinoline moiety, so that it will not form at all (scheme 4).



Scheme 4. Probable host–guest binding of HQNM and DHQ in the solution phase [18].

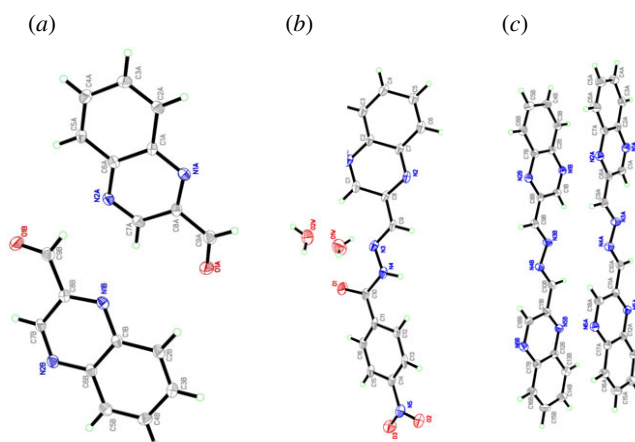


Figure 3. The molecular structures of (a) QA, (b) HQNM and (c) DHQ, showing 50% probability displacement ellipsoids for non-H atoms and the atom-numbering scheme.

2.1. X-ray crystallography

The X-ray structure of QA has been reported with a CCDC number CCDC 978283. For QA, the asymmetric unit consists of two molecules, with comparable geometries (figure 3a) which are approximately planar (for the 12 non-H atoms). There are no significant hydrogen bonds observed in the crystal structure, and molecules are stacked along the axis (electronic supplementary material, figure S5) by way of weak aromatic π – π stacking interactions between the benzene rings in adjacent molecules. The X-ray structure of HQNM has been reported with a CCDC number CCDC 1023223.

The compound HQNM (figure 3b) consists of a HQNM molecule and 1.5 water molecule in the asymmetric unit, and exists in trans conformations related to the $\text{N}3=\text{C}9$ bond. One of the water molecules lies in a mirror plane. The dihedral angle between the two benzene rings is $38.3(4)^\circ$. In the crystal, molecules are linked into two-dimensional planes (electronic supplementary material, figure S6) lying parallel to (10-1) via intermolecular $\text{C}-\text{H}\cdots\text{O}$ hydrogen bonds (electronic supplementary material, table S2). Adjacent planes are cross-linked via water molecules with further $\text{O}-\text{H}\cdots\text{O}$, $\text{N}-\text{H}\cdots\text{O}$ and $\text{C}-\text{H}\cdots\text{O}$ interactions into a three-dimensional network (electronic supplementary material,

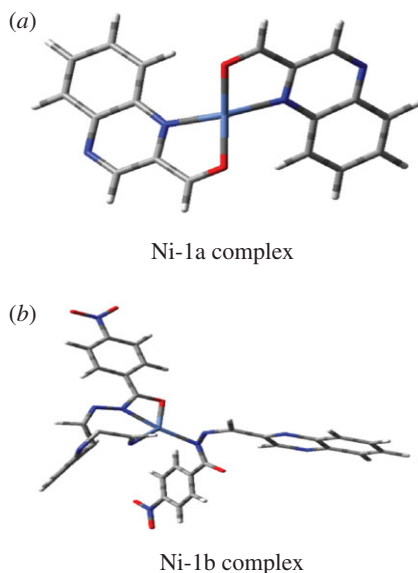


Figure 4. The structures of (a) Ni-QA (1a) and (b) Ni-HQNM (1b).

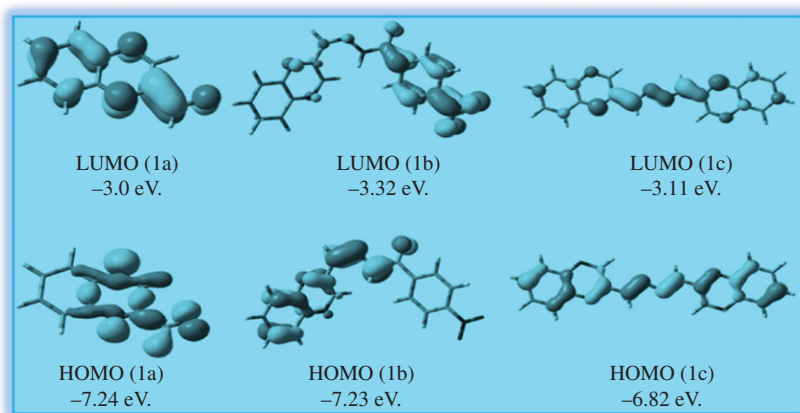


Figure 5. Frontier molecular orbital (HOMO and LUMO) of structures (1a) QA, (1b) HQNM and (1c) Quinoxaline DHQ with ISO value cut-off 0.04.

figure S6c). The crystal packing is further consolidated by π - π stacking interactions between the two symmetry-related benzene rings.

The asymmetric unit of DHQ (figure 3c) contains two crystallographically independent molecules, both of which exist in trans, trans conformations related to the N3=C9 and N4=C10 bonds. The non-H atoms of the monohydrazone quinoxaline moiety are nearly coplanar. The dihedral angle between the two quinoxaline rings within each molecule is 9.22 (6)° and 2.45 (6)°, respectively. In the crystal packing, adjacent molecules are linked via pairs of intermolecular C-H...N interactions, forming R22(8) ring motifs and, together with other intermolecular C...N interactions, assembled into chains propagating in [100]. Molecules are also stacked by π - π interactions between the pyrazine/pyrazine and benzene/benzene rings of adjacent sheets. The X-ray structure of DHQ has been reported with a CCDC number CCDC 977221.

2.2. Theoretical calculations

As in figure 4, DFT calculations were carried out using the Gaussian 03 (Revision B.04) [31–33] package. ‘Gauss View’ is used for visualization of molecular orbital (electronic supplementary material). The observation is that the compound QA (1a) does not bind with Ni²⁺. High dimerization stability of QA (1a) hydrogen bond formation and by the perfect stacking interactions with no steric crowding is the key reason for the formation of a highly stable stacked dimer. The calculated dimerization energy in

1a with that obtained from DFT calculations can be understood from the proposed less stable hindered chair forms of the nickel complex to the more open structure of the Ni–1a complex as shown above to be obtained by calculation.

High dimerization stability of 1a by hydrogen bond formation and by the perfect stacking interactions with no steric crowding is the key reason for the formation of a highly stable stacked dimer. The calculated dimerization energy in the case of 1a is 3.5 and 8 kcal mol⁻¹, respectively. The difference in the proposed complex structure of 1b with that obtained from DFT calculations can be understood from the proposed less stable hindered chair forms of the Ni²⁺ complex to the more open structure of the Ni–1b complex as shown above to be obtained by calculation (figure 5).

3. Conclusion

In conclusion, herein we report a new crystal structure for dimeric QA, HQNM and quinoxaline dihydrazone (DHQ). Among the three compounds, HQNM can selectively and successfully recognize nickel and DHQ recognizes Fe³⁺ cation selectively over other interfering cations in acetonitrile–HEPES buffer (9 : 1, v/v, pH = 7.4) solution, but QA cannot. The detection limits of Ni²⁺ and Fe³⁺ were found to be 1.47 μM and 1.60 × 10⁻⁵ M, respectively, from the absorption spectral change, which is sufficiently low and enables the detection of those cations in chemical and biological systems. The theoretical study of the three crystals along with the HOMO–LUMO calculation has also been shown.

Data accessibility. This article does not contain any additional data.

Authors' contributions. S.C. did the experiment and drafted the manuscript. S.G. analysed and critically revised the spectral data. C.K.Q. did the XRD experiment and analysed the data. B.P. did the theoretical calculation. S.G. did the revision work. All the authors gave their final approval for publication.

Competing interests. We have no competing interests.

Funding. This research has been funded by the DST-SERB (PDF/2016/002856).

Acknowledgements. We acknowledge DST-Science and Engineering Research Board (SERB) for funding under National Post-Doctoral Fellowship scheme (File no. PDF/2016/002856). S.C. thanks TCG Life sciences Ltd and Dr Sandipan Halder for spectral support and Prof. Sabyasachi Sarkar (Centre for Healthcare Science & Technology, Indian Institute of Engineering Science and Technology, Shibpur, Howrah) for helping in the initial drafting of the manuscript. S.C. also thanks Dr Sukdeb Pal (present mentor), Dr N. N. Rao (present Head of the Department, WWTD-NEERI-CSIR) and Dr Rakesh Kumar (Director, NEERI-CSIR), Nagpur, India for the opportunity to work in NEERI-CSIR. We gratefully thank TCG Life Sciences Ltd and Dr Sandipan Halder (Chemistry Department, VNIT-Nagpur) for help with spectral analysis.

References

- Loriga M, Piras S, Sanna P, Paglietti G. 1997 Quinoxaline chemistry. Part 7. 2-[aminobenzoates]- and 2-[aminobenzoylglutamate]-quinoxalines as classical antifolate agents: synthesis and evaluation of *in vitro* anticancer, anti-HIV and antifungal activity. *Farmaco* **52**, 157–166. (doi:10.1002/chin.199740197)
- Seitz LE, Suling WJ, Reynolds RC. 2002 Synthesis and antimycobacterial activity of pyrazine and quinoxaline derivatives. *J. Med. Chem.* **45**, 5604–5606. (doi:10.1021/jm020310n)
- Kim YB, Kim YH, Park JY, Kim SK. 2004 Synthesis and biological activity of new quinoxaline antibiotics of echinomycin analogues. *Bioorg. Med. Chem. Lett.* **14**, 541–544. (doi:10.1016/j.bmcl.2003.09.086)
- Hui X, Desrivot J, Bories C, Loiseau PM, Franck X, Hocquemiller R, Figadère B. 2006 Synthesis and antiprotazoal activity of some new synthetic substituted quinoxalines. *Bioorg. Med. Chem. Lett.* **16**, 815–820. (doi:10.1016/j.bmcl.2005.11.025)
- Lindsay CW *et al.* 2005 Allosteric Akt (PKB) inhibitors: discovery and SAR of isozyme selective inhibitors. *Bioorg. Med. Chem. Lett.* **15**, 761–764. (doi:10.1016/j.bmcl.2004.11.011)
- Labarbera DV, Skibo EB. 2005 Synthesis of imidazo[1,5,4-de]quinoxalin-9-ones, benzimidazole analogues of pyrroloiminoquinone marine natural products. *Bioorg. Med. Chem.* **13**, 387–395. (doi:10.1016/j.bmc.2004.10.016)
- Sarges R, Howard HR, Browne RG, Lebel LA, Seymour PA, Koe BK. 1990 4-Amino[1,2,4]triazolo[4,3-a]quinoxalines: a novel class of potent adenosine receptor antagonists and potential rapid-onset antidepressants. *J. Med. Chem.* **33**, 2240–2254. (doi:10.1021/jm00170a031)
- Galal SA *et al.* 2013 Design, synthesis and structure–activity relationship of novel quinoxaline derivatives as cancer chemopreventive agent by inhibition of tyrosine kinase receptor. *Eur. J. Med. Chem.* **69**, 115–124. (doi:10.1016/j.ejmech.2013.07.049)
- Sanna P, Carta A, Loriga M, Zanetti S, Sechi L. 1999 Preparation and biological evaluation of 6/7-trifluoromethyl(nitro)-, 6,7-difluoro-3-alkyl (aryl)-substituted-quinoxalin-2-ones. Part 3. *II Farmaco* **54**, 169–177. (doi:10.1016/S0014-827X(99)0011-7)
- Hui X, Desrivot J *et al.* 2006 Synthesis and antiprotazoal activity of some new synthetic substituted quinoxalines. *Bioorg. Med. Chem. Lett.* **16**, 815–820. (doi:10.1016/j.bmcl.2005.11.025)
- Shibinskaya MO, Lyakhov SA, Mazepa AV, Andronati SA, Turov AV, Zholobak NM, Spivak NYa. 2010 Synthesis, cytotoxicity, antiviral activity and interferon inducing ability of 6-(2-aminoethyl)-6H-indolo[2,3-b]quinoxalines. *Eur. J. Med. Chem.* **45**, 1237–1243. (doi:10.1016/j.ejmech.2009.12.014)
- Parra S *et al.* 2001 Imidazo[1,2-a]quinoxalines: synthesis and cyclic nucleotide phosphodiesterase inhibitory activity. *Eur. J. Med. Chem.* **36**, 255–264. (doi:10.1016/S0223-5234(01)01213-2)
- Burguete A *et al.* 2011 Synthesis and biological evaluation of new quinoxaline derivatives as antioxidant and anti-inflammatory agents. *Chem. Biol. Drug Des.* **77**, 255–267. (doi:10.1111/j.1747-0285.2011.01076.x)
- Dell A, Williams DH, Morris HR, Smith GA, Feeney J, Roberts GCK. 1975 Structure revision of the antibiotic echinomycin. *J. Am. Chem. Soc.* **97**, 2497–2502. (doi:10.1021/ja00842a029)
- Bailly C, Echebare S, Gago F, Waring M. 1999 Recognition elements that determine affinity and sequence-specific binding to DNA of 2QN, a

- biosynthetic bis-quinoline analogue of echinomycin. *Anti-Cancer Drug Des.* **15**, 291–303.
16. Sato S, Shiratori O, Katagiri K. 1967 The mode of action of quinoxaline antibiotics. Interaction of quinomycin A with deoxyribonucleic acid. *J. Antibiot.* **20**, 270–276.
 17. Potewar TM, Ingale SA, Srinivasan KV. 2008 Efficient synthesis of quinoxalines in the ionic liquid 1-*n*-butylimidazolium tetrafluoroborate ([Hbm]⁺BF₄⁻) at ambient temperature. *Synth. Commun.* **38**, 3601–3612. (doi:10.1080/00397910802054271)
 18. Goswami S, Chakraborty S, Paul S, Halder S, Maity AC. 2013 A simple quinoxaline-based highly sensitive colorimetric and ratiometric sensor, selective for nickel and effective in very high dilution. *Tetrahedron Lett.* **54**, 5075–5077. (doi:10.1016/j.tetlet.2013.07.051)
 19. Goswami S, Chakraborty S, Das AK, Manna A, Bhattacharyya A, Quah CK, Fun HK. 2014 Selective colorimetric and ratiometric probe for Ni(II) in quinoxaline matrix with the single crystal X-ray structure. *RSC Adv.* **4**, 20 922–20 926. (doi:10.1039/C4RA00594E)
 20. Goswami S, Chakraborty S, Adak MK, Halder S, Quah CK, Fun HK, Pakhira B, Sarkar S. 2014 A highly selective ratiometric chemosensor for Ni²⁺ in a quinoxaline matrix. *New J. Chem.* **38**, 6230–6235. (doi:10.1039/C4NJ01498G)
 21. Denkhaus E, Salkinow K. 2002 Nickel essentiality, toxicity, and carcinogenicity. *Crit. Rev. Oncol. Hematol.* **42**, 35–56. (doi:10.1016/S1040-8428(01)00214-1)
 22. Wang HX, Wang DL, Wang Q, Li XY, Schalley CA. 2010 Nickel(II) and iron(III) selective off-on-type fluorescence probes based on perylene tetracarboxylic diimide. *Org. Biomol. Chem.* **8**, 1017. (doi:10.1039/b921342b)
 23. Kim WY, Shi H, Jung HS, Cho D, Verwilt P, Lee JY, Kim JS. 2016 Coumarin-decorated Schiff base hydrolysis as an efficient driving force for the fluorescence detection of water in organic solvents. *Chem. Commun.* **52**, 8675–8678. (doi:10.1039/C6CC04285F)
 24. Connor A, Hu T, Detchou C, Liu R, Pulavarti SV, Szyperski T, Lu Z, Gong B. 2016 Aromatic oligureas as hosts for anions and cations. *Chem. Commun.* **52**, 9905–9908. (doi:10.1039/C6CC03681C)
 25. Brown A, Beer PD. 2016 Halogen bonding anion recognition. *Chem. Commun.* **52**, 8645–8658. (doi:10.1039/C6CC03638D)
 26. Antonisse MG, Reinhoudt DN. 1998 Neutral anion receptors: design and application. *Chem. Commun.* **4**, 443–448. (doi:10.1039/a707529d)
 27. Wang J, Zhang D, Liu Y, Ding P, Wang C, Ye Y, Zhao Y. 2014 A N-stabilization rhodamine-based fluorescent chemosensor for Fe³⁺ in aqueous solution and its application in bioimaging. *Sens. Actuators, B* **191**, 344–350. (doi:10.1016/j.snb.2013.10.018)
 28. Choi YW, Park GJ, Na YJ, Jo HY, Lee SA, You GR, Kim C. 2014 A single schiff base molecule for recognizing multiple metal ions: a fluorescence sensor for Zn(II) and Al(III) and colorimetric sensor for Fe(II) and Fe(III). *Sens. Actuators, B* **194**, 343–352. (doi:10.1016/j.snb.2013.12.114)
 29. Xu JH, Hou YM, Ma QJ, Wu XF, Wei XJ. 2013 A highly selective fluorescent sensor for Fe³⁺ based on covalently immobilized derivative of naphthalimide. *Spectrochim. Acta A* **112**, 116–124. (doi:10.1016/j.saa.2013.04.044)
 30. Reddy G, Lo R, Roy S, Banerjee T, Ganguly B, Das A. 2013 A new receptor with a FRET based fluorescence response for selective recognition of fumaric and maleic acids in aqueous medium. *Chem. Commun.* **49**, 9818–9820. (doi:10.1039/c3cc45051a)
 31. Frisch MJ et al. 2004 *Gaussian 03, revision C.02*. Wallingford, CT: Gaussian, Inc.
 32. Hay PJ, Wadt WR. 1985 *Ab initio* effective core potentials for molecular calculations: potentials for K to Au including the outermost core orbitals. *J. Chem. Phys.* **82**, 299–310. (doi:10.1063/1.448975)
 33. Hay PJ, Wadt WR. 1985 *Ab initio* effective core potentials for molecular calculations: potentials for the transition metal atoms Sc to Hg. *J. Chem. Phys.* **82**, 270–283. (doi:10.1063/1.448799)